JOURNAL OF CATALYSIS 152, 1–17 (1995)

Preparation, Characterization, and Catalytic Properties of VAPO-5 for the Oxydehydrogenation of Propane

T. Blasco, P. Concepción, J. M. López Nieto,[1] and J. Pérez-Pariente[2]

Instituto de Tecnología Química UPV-CSIC, Universidad Politécnica de Valencia, Camino de Vera s/n, 46071-Valencia, Spain

Received June 8, 1994; revised October 21, 1994

Vanadium aluminophosphates with AFI structure (VAPO-5) have been prepared by hydrothermal synthesis, characterized by several physicochemical techniques (i.e., thermogravimetric analysis, XRD, Solid state MAS NMR, UV–Vis, EPR, TPR), and tested for the oxidative dehydrogenation of propane. The influence of the different synthesis parameters, particularly the content and oxidation state of vanadium, the pH of the gel, and the presence of complexing agents, has been studied. The vanadium atom are incorporated as isolated vanadyl VO^{2+} ions in square pyramidal or distorted octahedral environments. After calcination in air, most of the V^{4+} ions are oxidized to V^{5+} in square pyramidal or octahedral symmetry, which evolve toward tetrahedral coordination upon dehydration. The VAPO-5 samples are active and selective for the oxidative dehydrogenation of propane. Their catalytic properties are better than the corresponding $ALPO_4$-5 supported vanadium catalysts. Isolated tetrahedral V^{5+} species in the framework of AFI structure are proposed to be the active and selective sites for the oxydehydrogenation of propane. © 1995 Academic Press, Inc.

1. INTRODUCTION

Supported vanadium oxides are industrially important catalysts for the selective oxidation of hydrocarbons (1–3). In the case of the oxidative dehydrogenation (ODH) of propane, vanadium supported on MgO presents a high selectivity (4–6), while when supported on Al_2O_3, TiO_2, or SiO_2 it gives low selectivity to propene (7). Recently, it has been proposed that the better catalytic properties of V–Mg–O catalysts for the oxidative dehydrogenation of alkanes are due to the formation of isolated VO_4 tetrahedra on the surface of MgO (6).

An attractive alternative to supported catalysts can be the use of transition metal substituted molecular sieves, which allow one to obtain well-defined and dispersed active sites. In this way, V–silicalite (8, 9) and VAPO-5 (10) have been reported to be selective catalysts for the oxidative dehydrogenation of propane.

The vanadium aluminophosphate VAPO-5 has been prepared by different methods (11–16) but the nature and sitting of vanadium species is still under discussion. Thus, tetrahedral vanadium species substituting phosphorus positions (12, 13) and monomeric vanadyl units in square pyramidal or distorted octahedral vanadium species in a phosphate environment (16) have been proposed.

On the other hand, little information on the catalytic properties of VAPO-5 has been published. Interesting catalytic properties have been observed for the oxidation of hydrocarbons in liquid phase (16–17) and for the catalytic dehydrogenation of ethylbenzene (18). In the case of oxidation reactions using molecular oxygen, VAPO-5 presents a low selectivity for the amoxidation of propane (15) or the oxidation of toluene (17) but it shows a high selectivity for the ODH of propane (10).

The aim of the present paper is the study of the nature and catalytic properties of vanadium species in VAPO-5. In this way, several samples of this material have been prepared in a broad range of conditions and characterized by different methods. In addition, the catalytic properties of VAPO-5 for the oxidative dehydrogenation of propane have been studied.

2. EXPERIMENTAL

Synthesis

VAPO-5 samples were synthesized hydrothermically from gels with the following molar composition:

$$P_2O_5 : 0.8\ Al_2O_3 : xV_2O_5 : 1.76\ TEA : 47\ H_2O : y\ A$$

(A, oxalic acid, hydrazine, H_2SO_4, HF).

The reagents used were orthophosphoric acid (Riedel, 85 wt%), pseudobohemite (Catapal B Vista, 70 wt% Al_2O_3), triethylamine, TEA, (ALDRICH, 99 wt%), and V_2O_5 (Merck). V^{4+}-containing solutions, obtained from stoichiometric reduction of V_2O_5 by hydrazine or oxalic acid, were used in most cases. V_2O_5 was also used in one

[1] To whom correspondence should be addressed.

[2] Present address: Instituto de Catálisis y Petroleoquímica, Campus UAM-Cantoblanco, 28049-Madrid, Spain.

0021-9517/95 $6.00

TABLE 1

Preparation Procedures of Vanadium Aluminophosphates

Series	Reductor	Complexing anion	H_2SO_4/reductor molar ratio
A[a]	Oxalic acid	Oxalate	—
B0[b]	Oxalic acid	F^-	0
B2[c]	Oxalic acid	F^-	2
C4[d]	Hydrazine	—	4
C5[d]	Hydrazine	—	5
C10[d]	Hydrazine	—	10
D[e]	—	—	—

[a] Oxalic acid/V_2O_5 molar ratio of 3.
[b] Oxalic acid/fluorhydric acid/V_2O_5 molar ratio of 1.2/4.2/1.
[c] Oxalic acid/fluorhydric acid/V_2O_5 molar ratio of 1/4/1.
[d] Hydrazine/V_2O_5 molar ratio of 0.5.
[e] V_2O_5 was incorporated directly in gel in a triethylamine solution (V_2O_5/ET_3N molar ratio of 0.267).

preparation. HF and/or H_2SO_4 were also added to the synthesis gel. Full descriptions of the preparation procedure and the chemical composition of the synthesis gel are given in Tables 1 and 2, respectively. It must be noted that oxalate and fluoride anions can form complexes with vanadyl VO^{2+} cations.

The synthesis procedure was as follows:

$$H_3PO_4 + H_2O \xrightarrow[\text{2 h (rt) stirring}]{Al_2O_3+H_2O} \xrightarrow[\text{2 h (rt) stirring}]{\text{TEA}} \xrightarrow[\text{2 h (rt) stirring}]{\text{vanadium solution}} \text{Gel}$$

(rt) = Room Temperature

The reaction mixture obtained was introduced in 60 ml PTFE-lined stainless steel autoclaves and heated at 200°C for 16 h. After this, the autoclaves were quenched in cool water, centrifuged at 10,000 rpm, and washed and dried at 80°C. A portion of the solid product was calcined in air at 550°C for 8 h (Table 2).

For comparison purposes, supported vanadium catalysts were prepared by impregnation of $ALPO_4$-5 with aqueous solutions of vanadyl oxalate, according to the procedure described previously (19). The samples were dried at 80°C overnight and further calcined in air at 550°C for 8 h.

VAPO-5 (referred to as A, B, C, D) and ALPO-5 supported vanadium catalysts (referred as V/ALPO) are preceded by a number that indicates the wt% of atomic vanadium.

TABLE 2

Vanadium Content and Crystallinity of the Different Samples

Sample[a]	V/(Al + P) atomic ratio		Vanadium content[b] (wt%)	Yield of VAPO-5 (%)[c]	Crystallinity (%)[d]	
	In gel	In catalysts			Before calcination	After calcination
0.41-A	0.008	0.006	0.41	12.6	100	98
0.38-A	0.016	0.005	0.38	13.5	94	99
1.0-A	0.065	0.015	1.00	16.1	90	54
1.2-A	0.131	0.020	1.22	12.2	96	89
0.8-BO	0.065	0.012	0.75	10.8	96	58
1.4-B2	0.065	0.020	1.41	—	93	52
2.0-C4	0.044	0.028	2.02	14.3	100	87
2.5-C4	0.065	0.036	2.52	11.7	100	99
3.1-C4	0.131	0.049	3.09	11.8	76	Trydimite
1.6-C5	0.065	0.023	1.59	15.4	82	56
5.7-C5	0.131	0.087	5.72	5.4	45	Trydimite + V_2O_5
6.4-C10	0.065	0.107	6.40	15.9	47	Trydimite + V_2O_5
0.5-D	0.065	0.006	0.47	10.3	90	83

[a] A, B, C, D indicate the preparation procedure in Table 1.
[b] Vanadium content in calcined samples, as wt% of V atoms.
[c] Obtained after 16 h.
[d] The crystallinity is referred from uncalcined $ALPO_4$-5.

Characterization

Chemical analysis of Al and V was conducted by atomic absorption, and P was determined by a colorimetric method using the complex formed between phosphorus and molybdovanadic acid.

X-ray diffraction (XRD) was performed on a Phillips 1060 diffractometer provided with graphite monochromator employing nickel-filtered Cu$K\alpha$ radiation (λ = 0.1542 nm). Crystallinity was determined by measuring the intensity of the peaks appearing at $2\Theta \approx 19.8$, 21.1, and 22.4 and comparing them with the uncalcined $ALPO_4$-5.

Thermogravimetric (TG) analysis and differential thermal analysis (DTA) were performed on a Netzsch STA-409EP instrument in the temperature range 20–800°C with a 0.02 g sample. The heating rate was 10°C min^{-1} and the air flow 100 ml min^{-1}.

Scanning electron microscopy (SEM) and EDAX microanalysis were performed on an ISI 1300 instrument.

Solid state ^{27}Al, ^{31}P, and ^{51}V-NMR spectra were recorded at ambient temperature on a Varian VXR-400 S WB spectrometer at 100.6, 161.9, and 105.1 MHz, respectively. A high speed MAS Doty probe with zirconia rotors (5 mm in diameter) was used. ^{27}Al spectra were obtained with a 0.6-μs pulse length corresponding to a flip angle of $\pi/20$ and a recycle delay of 0.5 s. For ^{31}P, a pulse of 3 μs equivalent to a $3\pi/8$ flip angle and a recycle delay of 15 s were used. The samples were spun at a rate of 7 KHz to record the NMR spectra of ^{27}Al and ^{31}P. The cross polarization experiments on ^{31}P and ^{27}Al were carried out by using $\pi/2$ pulses for protons of 5.5 and 7 μs, respectively. The contact times used were 1.5 ms for ^{31}P and 0.8 ms for ^{27}Al. ^{51}V NMR spectra were recorded with pulses of 1 μs (flip angle $\pi/13$) and 1 s repetition time. The number of scans accumulated was around 60,000. The obtained free induction decays were multiplied by an exponential 500-Hz line broadening in order to decrease the noise in the spectra. All chemical shifts are referenced against liquid $VOCl_3$, using a 0.16 *M* $NaVO_3$ aqueous solution as secondary reference, whose chemical shift is −574.28 ppm.

Diffuse reflectance (DR) spectra in the UV–Visible region were collected with a Shimazdu UV-2010 PC spectrophotometer equipped with a reflectance attachment. Different reference compounds, such as V_2O_5, and NH_4VO_3 commercial products and MgO supported vanadium samples (11 wt% of vanadium atom) (20) were used.

The ESR spectra were recorded at 77 K in the Brucker ER-200 spectrometer at X-Band. DPPH (g = 2.0036) was used as a standard to calibrate the g value scale.

TPR results were obtained in a Micromeritics apparatus. Samples of 100 mg were first treated in argon at room temperature for 1 h. The samples were subsequently contacted with an H_2/Ar mixture (H_2/Ar molar ratio of 0.15 and a total flow of 50 ml min^{-1}) and heated, at a rate of 10°C min^{-1}, to a final temperature of 1000°C.

Catalytic Test

The catalytic tests for the oxidative dehydrogenation of propane were carried out in a fixed bed quartz tubular reactor (16 mm i.d., 500 mm length) equipped with a coaxial thermocouple for temperature profiles.

Catalyst samples from 0.5 to 1.7 g and particle sizes between 0.25 and 0.42 mm were mixed with variable amounts of SiC (0.59 mm particle size) to keep a constant volume in the catalyst bed (3 cm^3). The reaction was studied in the temperature interval 450–540°C using a propane/oxygen/helium molar ratio of 4/8/88. The total flow was varied from 100 to 200 ml min^{-1} obtaining different contact times (W/F = 40 to 175 g_{cat} h (mol C_3)$^{-1}$).

Analyses of reactants and products were carried out by gas chromatography, using two column types: (i) Porapak Q (3.0 m × $\frac{1}{8}$ in.); (ii) molecular sieve 5A (1.5 × $\frac{1}{8}$ in.).

Blank runs in the temperature interval 450–600°C were carried out substituting the catalyst by SiC at the low total flow used (100 ml min^{-1}) in the present study. Under our reaction conditions the presence of homogeneous reaction can be neglected.

3. RESULTS

Synthesis of VAPO-5

The influence of the different synthesis parameters on the nature of the solid phases obtained has been studied, particularly the content and oxidation state of vanadium (V^{4+} and V^{5+}), the pH of the gel, and the presence of complexing agents like oxalate and fluoride anions. The vanadium content and crystallinity of the uncalcined and calcined samples are collected in Table 2. In the uncalcined samples, AFI was the only crystalline phase detected by XRD. However, the crystallinity changes as a function of the specific synthesis conditions and remains higher than about 90% up to a vanadium content of 3 wt%, decreasing for higher vanadium content (Fig. 1A). This vanadium content corresponds to ~1.2 vanadium atom per unit cell (V/u.c.).

For the crystalline products, the unit cell parameters change with the vanadium content as indicated in Fig. 2, following the a and c parameters opposite trends. This causes the unit cell volume to increase by about 1% in the range here studied.

However, no change in unit cell parameters of uncalcined VAPO-5 is reported in Refs. (12) and (16), probably due to the small vanadium content of these samples. Other authors have reported changes of a and c parameters of the order of 0.01–0.02 Å, for vanadium content lower than 1%, when tripropylamine was used as template (13, 14).

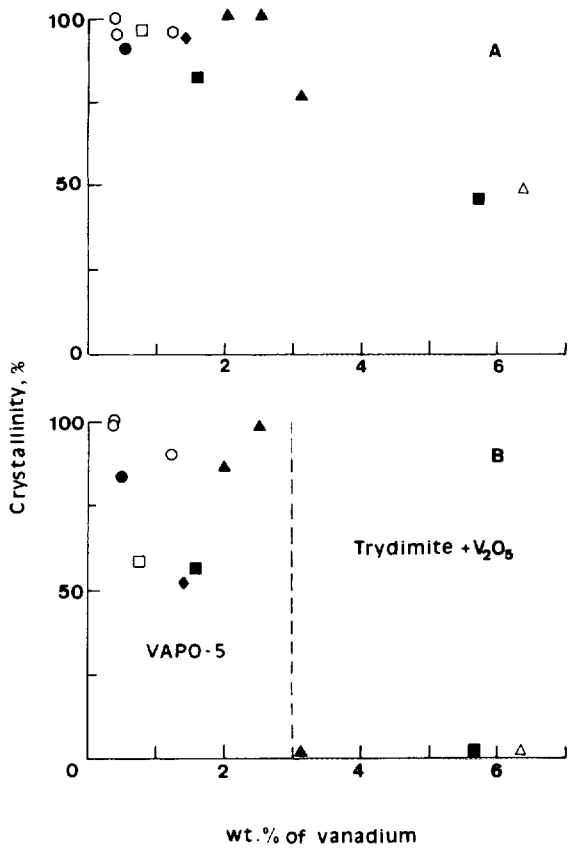

FIG. 1. Influence of the vanadium content on the crystallinity of as-synthesized (A) and calcined (B) VAPO-5 samples: (○) A series, (□) BO series, (♦) B2 series, (▲) C4 series, (■) C5 series, (△) C10 series, and (●) D series.

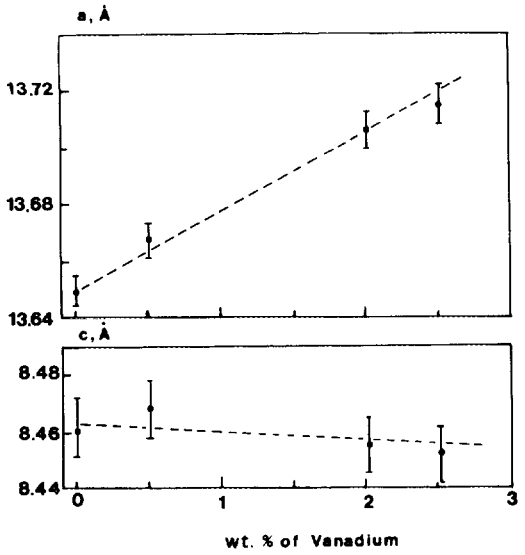

FIG. 2. Variation of the *a* and *c* cell parameters with the vanadium content of VAPO-5.

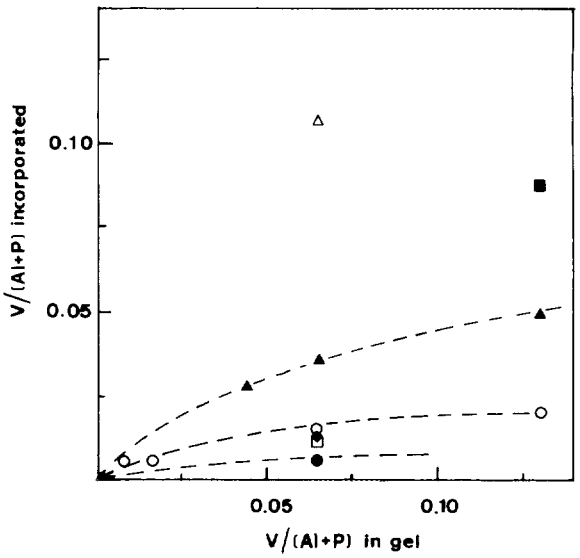

FIG. 3. Variation of the incorporation of vanadium in vanadium aluminophosphates with the vanadium content in the synthesis gel. Symbols are as in Fig. 1.

The amount of vanadium incorporated into the crystals depends in a complex manner on the composition of the synthesis mixtures. First, the samples prepared from V^{4+} have a higher metal content than the corresponding 0.5-D sample (prepared from V^{5+}). As a consequence, the efficiency in vanadium incorporation is very low in this last case, and only about 5% of the total metal is found in the crystals of VAPO-5. Second, the vanadium content in the solid products increases with its concentration in the synthesis gel, the other parameters being constant. However, the efficiency in vanadium incorporation decreases also in this order (Table 2). This behavior is depicted in Fig. 3 for samples crystallized in absence and in presence of oxalate. The presence of the complexing anions (F^- or $C_2O_4^{2-}$) in the solution clearly decreases the degree of vanadium incorporation into the crystals (Table 2).

In contrast, the vanadium content of the solids can be enhanced by decreasing the pH of synthesis (samples 3.1-C4 and 5.7-C5, and 2.5-C4 and 6.4-C10, respectively). However, this results in poorly crystalline solids (Fig. 1A).

The stability of the crystals after calcination depends on their vanadium content: up to about 3 wt% of vanadium, the crystallinity loss is less than ~15%, provided that F^- is absent in the synthesis mixture (B series) or the H_2SO_4/reductor molar ratio is lower than 5 (1.5-C5 sample). Higher metal loading leads to the disappearance of the AFI phase and the formation of dense phases of trydimite-type and V_2O_5 crystallites (Fig. 1B). It must be noted that the use of acid in excess of that required by

TABLE 3

SEM–EDAX Results Obtained on Vanadium Aluminophosphates

Sample	EDAX analysis[a]	Crystal sizes (μm)
0.38-A	—	3.6
0.5-D	$P_{0.51}:Al_{0.49}:V_{0.007}$	0.97
1.0-A	$P_{0.51}:Al_{0.47}:V_{0.010}$	—
1.4-B2	$P_{0.51}:Al_{0.48}:V_{0.015}$	—
1.6-C5	$P_{0.51}:Al_{0.47}:V_{0.022}$	1.2

[a] P : Al : V atomic ratio.

the reduction stoichiometry of V^{5+} to V^{4+} results in a sample less stable against calcination (sample 1.6-C5).

These results suggest that the low stability of the VAPO-5 sample described in Ref. (16) might be due to the presence of an F^- anion in the synthesis gel.

Electron Microscopy

Crystals of VAPO-5 appear as hexagonal plates under the scanning microscopy (Fig. 4), quite uniform in size, which ranges from ~1 to ~4 μm, depending on the synthesis conditions (Table 3). However, in samples obtained from fluoride-containing gels a heterogeneous crystal size was obtained (Fig. 4b).

Microprobe analysis shows a very homogeneous vanadium distribution among different crystals, the metal content matching that determined by bulk chemical analysis.

Thermal Analysis

TG and DTA patterns of some selected samples are given in Fig. 5. Three different weight losses were detected in the 20–80, 80–220, and 220–630°C temperature ranges. The first two steps correspond to endothermic processes; the low temperature one is associated to water desorption and the second one to triethylamine desorption. The third exothermic step corresponds to combustion of some organic species occluded in the VAPO-5 cavities. The weight loss related to this exothermic step increases when increasing the vanadium content, whereas the TEA desorption decreases. At the same time the exothermic desorption occurs at higher temperatures, which are quite close to those observed for metal substituted $ALPO_4$-5 (21). This is usually taken as a proof that charge deficiency has been induced in the framework by isomorphous substitution. Montes *et al.* (12) observed that the exothermic step occurs at lower temperature for VAPO-5 than $ALPO_4$-5 when tripropylamine is used as template. However, other authors (13, 14) have also observed that the triethylamine molecules are strongly bonded in VAPO-5. This effect can be explained by the charge centers created by the V^{4+} ions in the framework. Then, it can be concluded that the exotherm process can be assigned to the combustion of protonated triethylamine ($TEAH^+$).

The weight losses, associated to the template degradation in the different temperature ranges, are collected in Table 4. It can be seen that the total organic content is approximately constant and equal to ~10 ± 1 wt%. This value corresponds to ~1.6 molecules of TEA per unit cell.

The exothermic weight loss has been corrected for the small contribution of the occluded nonprotonated organics; the $AlPO_4$-5 is taken as a reference. The resulting amount of organics is plotted in Fig. 6 as a function of the vanadium content. From the slope of the line it can be seen that the $TEAH^+/V$ ratio decreases from ~2 to close to 1 when increasing the vanadium loading.

In addition to this, TG patterns of VAPO-5 calcined samples were also obtained. In all cases, the presence of an endothermic peak at temperatures lower than 200°C was observed. This peak, which corresponds to a weight loss of ~15 wt%, is associated to water desorption and indicates that VAPO-5 rehydrates at room temperature. A similar effect has been observed by Rigutto and Van Bekkum (16).

Solid State NMR Spectroscopy

^{51}V NMR spectra. Previous solid state ^{51}V NMR studies on V-containing catalysts (16, 22–27) have shown that it is possible to obtain information on the symmetry environment of ^{51}V by comparison with model compounds. The ^{51}V isotope has a moderately large nuclear electric quadrupole moment, and the line shape of the wideline spectra are dominated by chemical shift anisotropy rather than second-order quadrupole effects (22–24). Extensive studies on V^{5+} model compounds show that more reliable information is obtained from static NMR spectra than from isotropic chemical shift obtained under MAS conditions (23–27).

Figure 7 shows the wideline ^{51}V NMR spectra of calcined vanadium aluminophosphate samples (0.38-A, 2.0-C4, 1.6-C5 and 0.5-D). All of them are mainly formed by a relatively broad line centered at around −300 ppm. Due to the low vanadium content of the samples the signal to noise ratio in the spectra is quite low and it is not possible to distinguish the other components of the shielding tensor. On the bases of previous studies on the relationship existing between the local symmetry of the vanadium sites and the ^{51}V wideline NMR spectra (22–27), the spectra obtained for the VAPO-5 samples can be interpreted as due to V atoms in distorted square pyramidal or octahedral environment. An additional line centered at around −510 ppm is observed in the spectrum of the 1.6-C5 sample, suggesting the presence of some tetrahedral vanadium. In fact, the existence of small amounts of vanadium in tetrahedral coordination cannot completely be ruled out in all the samples.

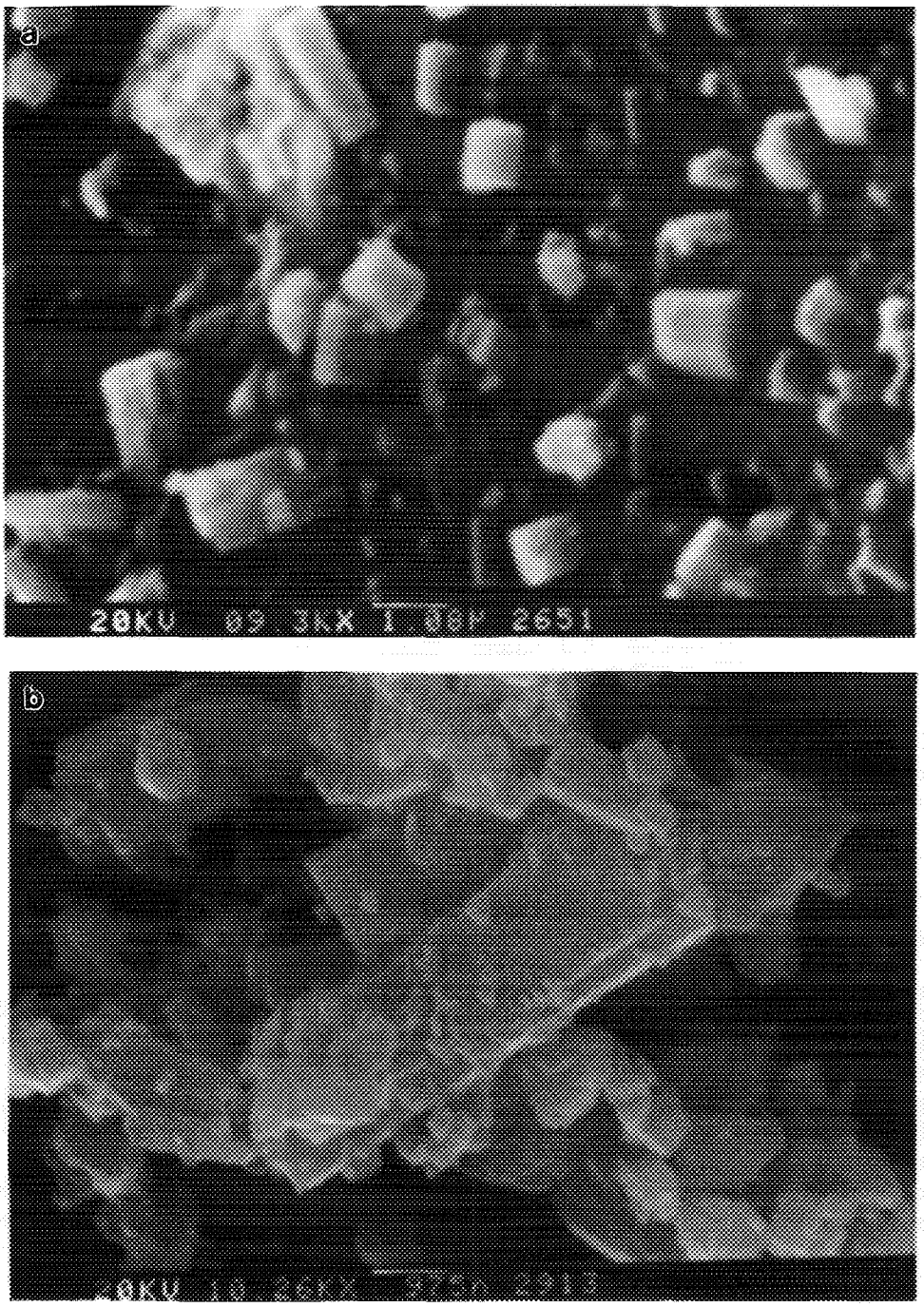

FIG. 4. SEM micrographs of calcined vanadium aluminophosphates. Samples: (a) 0.5-D, (b) 1.4-B2, and (c) 1.6-C5.

^{27}Al and ^{31}P MAS NMR spectra. The ^{27}Al MAS NMR spectra of the uncalcined and calcined 1.6-C5 samples are shown in Figs. 8a and 8b, respectively. The spectra are constituted by three peaks, and the only differences in the relative intensity of the lines constituting the spectra were found for the ALPO-5 and VAPO-5 samples studied in the present work. The main line at around 36 ppm is typical for tetrahedral aluminum in aluminophosphate frameworks (28–36). No influence of the presence of other heteroatoms in the second coordination shell of ^{27}Al is usually observed in the ^{27}Al MAS NMR spectra (29–31, 34, 36). Two additional resonances, which have also been previously observed in aluminophosphate or SAPO's materials, are present at −12 and 10 ppm approximately

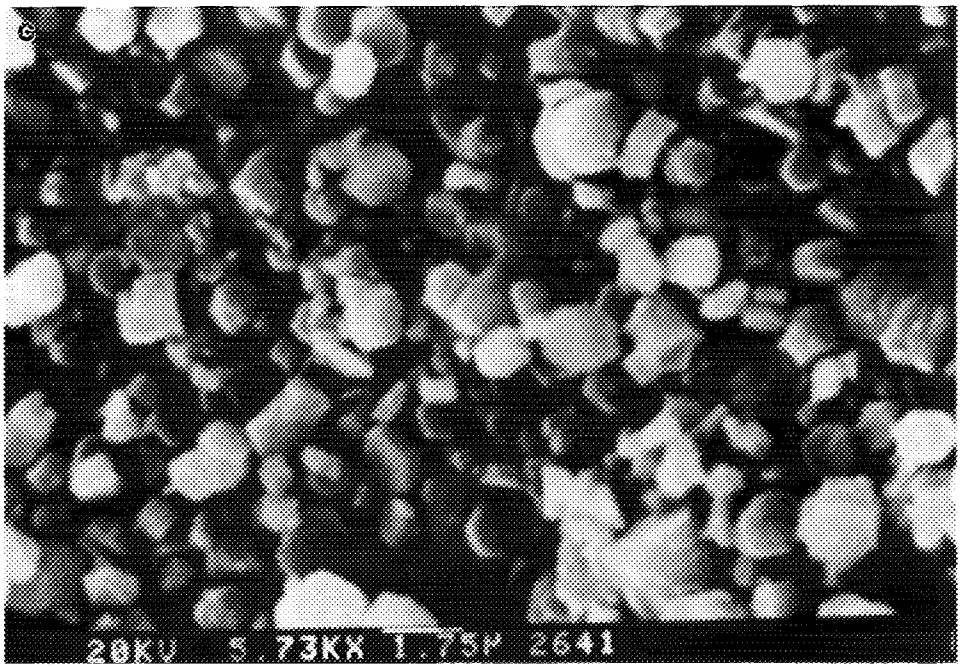

FIG. 4—*Continued*

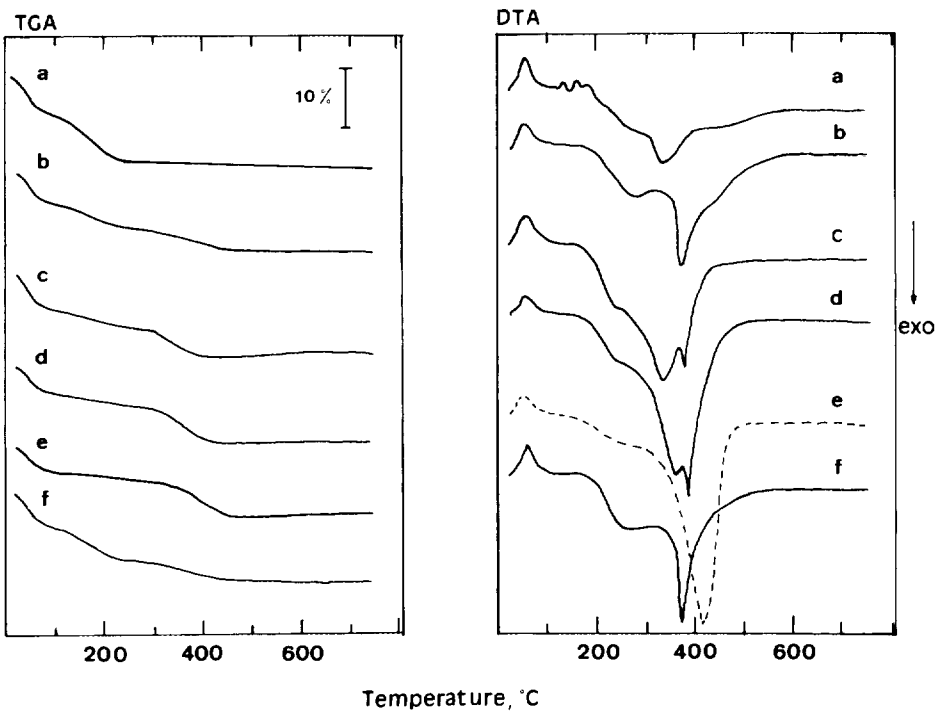

FIG. 5. TG and DTA patterns of as-synthesized vanadium aluminophosphates: (a) $ALPO_4$-5, (b) 0.41-A, (c) 1.2-A, (d) 2.0-C4, (e) 2.5-C4, and (f) 0.5-D.

TABLE 4

TG/DTA Results of Vanadium Aluminophosphates

Sample	Organic weight loss (wt%)		Total weight loss (wt%)
	Endothermic	Exothermic	
ALPO-5	8.55	2.93	11.5
0.41-A	5.49	4.38	9.9
0.38-A	5.53	5.38	10.7
0.5-D	6.41	4.59	11.0
1.2-A	3.55	5.47	9.0
2.0-C4	3.46	6.93	10.4
2.5-C4	2.05	6.76	8.8

(28–35). The ^{27}Al MAS NMR spectra recorded using cross polarization (CP) from protons are reported in Figs. 8c and 8d. The behavior of the uncalcined sample in the CP experiment (Fig. 8c) will be commented on below. The line at −12 ppm, in the resonance region of octahedrally coordinated aluminum, strongly increases when using ^{1}H–^{27}Al CP for calcined 1.6-C5 sample (Fig. 8d), indicating the presence of proton or water molecules in its neighborhood. This peak has been previously attributed (29, 33, 35) to framework tetrahedral aluminum coordinated to two additional water molecules in the calcined materials or to water or template in the uncalcined one. The assignment of the line at 10 ppm is still controversial (28, 29, 32–34). This peak, intermediate between tetrahedral and octahedral aluminum resonance peaks, is more enhanced than the tetrahedral aluminum peak by cross polarization from protons (see Figs. 8b and 8d). This observation and the chemical shift value have led some authors (28, 29, 32, 33) to assign this line to tetrahedral framework aluminum interacting with template or water molecules in the channels, in a trigonal–bipyramidal coordination in the aluminophosphate framework. This same line has also been assigned to unreacted pseudobohemite remaining after synthesis (34).

From comparison of spectra in Fig. 8, it is evident that the ^{1}H–^{27}Al CP is much less effective in the uncalcined 1.6-C5 sample, especially for the line at −12 ppm corresponding to tetrahedral aluminum linked to two extra tem-

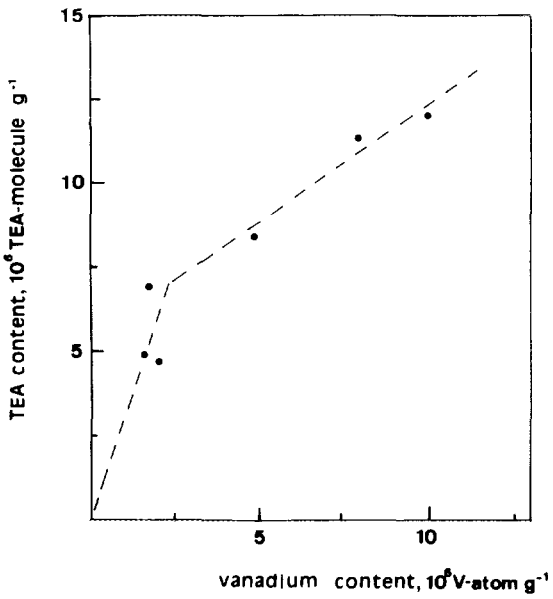

FIG. 6. Influence of the vanadium content on the triethylamine content determined by TG–DTA.

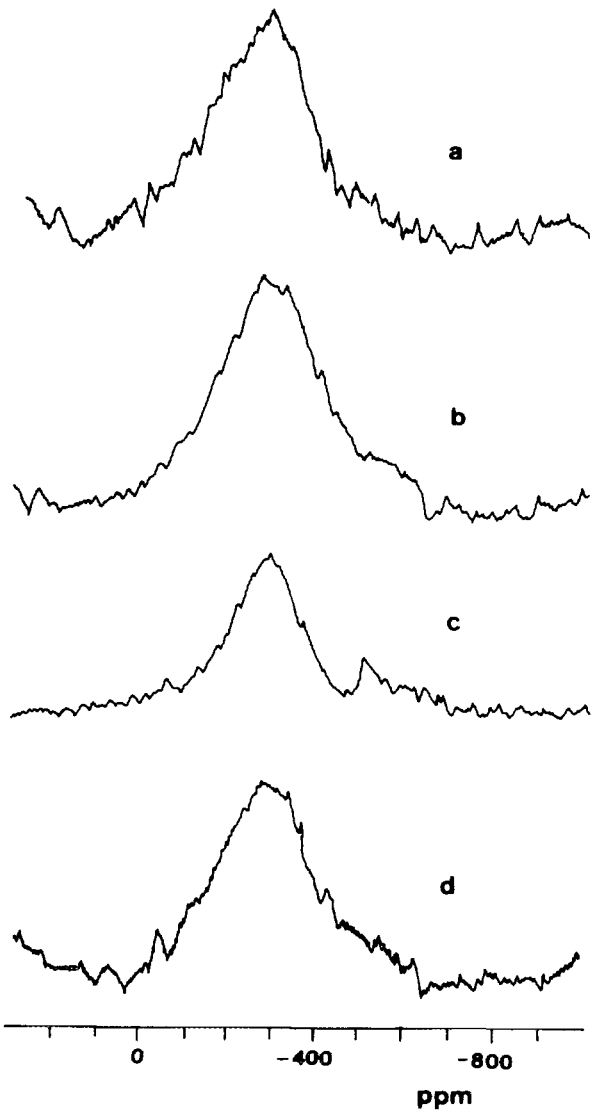

FIG. 7. ^{51}V NMR spectra of calcined vanadium aluminophosphates. Samples: 0.38-A (a), 2.0-C4 (b), 1.6-C5 (c), and 0.5-D (d).

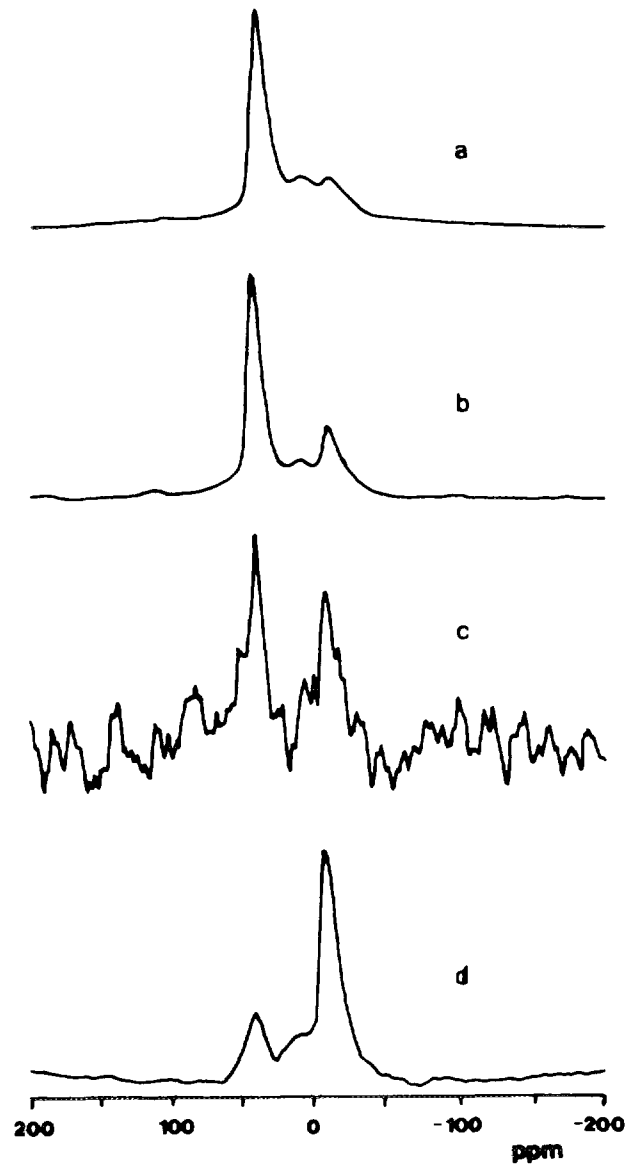

FIG. 8. ^{27}Al MAS NMR (a, b) and ^{1}H–^{27}Al cross polarization MAS NMR (c, d) spectra of uncalcined (a, c) and calcined (b, d) 1.6-C5 samples.

plate or water molecules. This effect has not been observed on sample 0.5-D (synthesized from V^{5+}), which behaves similarly to calcined 1.6-C5, both in the uncalcined and calcined states. In this sense, it is known that the presence of paramagnetic impurities can make the CP experiment uneffective (37). Sample 1.6-C5 was prepared from paramagnetic V^{4+} and thus the NMR results are in agreement with the presence of V^{4+} in the uncalcined material. After calcination, most of the V^{4+} are oxidized to V^{5+} (diamagnetic) and the polarization transfer from ^{1}H to ^{27}Al occurs, mostly increasing the lines corresponding to aluminum species interacting with protons.

The ^{31}P MAS NMR spectra of vanadium aluminophosphates are mainly formed by a line at around −29 ppm, which is characteristic of tetrahedral phosphorus in a $P-(O-Al)_4$ environment (29–36). Except for small differences, the spectra of the ALPO-5 and the VAPO-5's studied here are similar. The uncalcined materials present a shoulder to high frequency slightly increasing upon CP which is not visible after calcination, suggesting that it arises from framework phosphorus adjacent to occluded organic template molecules (36).

Diffuse reflectance spectra. The DR spectra of reference compounds, such as V_2O_5 and NH_4VO_3, and an MgO supported vanadium sample are shown in Fig. 9.

It is known that the lower-energy charge-transfer (LCT) bands for the vanadium ions, which are associated with oxygen to vanadium charge transfer, are stronly influenced by the coordination and/or the oxidation state of vanadium ions (20, 22, 38, 39). Thus, while the absorption bands for vanadium (V^{5+}) ions are observed in the 260–500-nm region, they appear in the 260–220-nm region for vanadium (V^{4+}) ions. In addition to this, a relationship between the coordination of vanadium (V^{5+}) ions and the position of the LCT absorption band has been proposed: the greater the coordination of vanadium the higher the wavenumber is. On the other hand, the presence of vanadium (V^{4+}) ions can be also observed in the 550–850 nm region due to the *d–d* transition of vanadium V^{4+} (d^1) ions.

The CT band at ca. 450 nm is the most characteristic of the DR spectrum of V_2O_5 (Fig. 9a) and has been tentatively attributed to charge transfer to a delocalized acceptor site, such as those on VO_6 chains (21). Polymeric V^{5+}

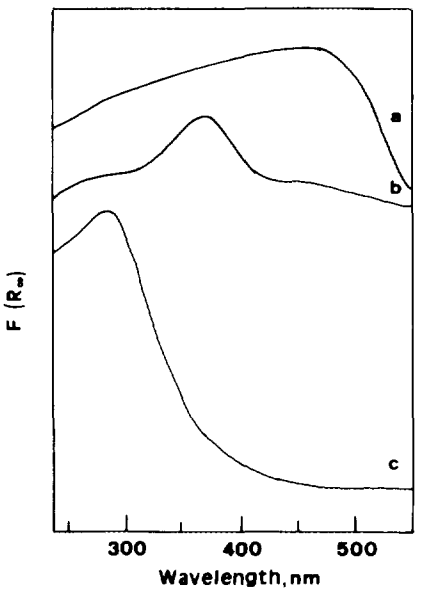

FIG. 9. DR spectra of: (a) V_2O_5, (b) NH_4VO_3, and (c) MgO supported vanadium sample (11 wt.% of vanadium).

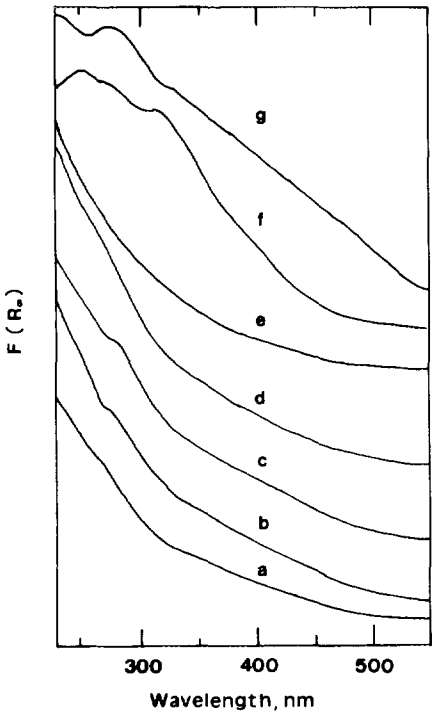

FIG. 10. DR spectra of calcined vanadium aluminophosphates: (a) 0.41-A, (b) 1.0-A, (c) 1.4-B2, (d) 1.6-C5, (e) 2.0-C4, (f) 2.5-C4, and (g) 6.4-C10.

species in a tetrahedral site symmetry, as in ammonium metavanadate NH_4VO_3, gives two CT bands at 290 and 360 nm (Fig. 9b). Figure 9c shows the DR spectrum of a MgO supported vanadium sample in which vanadium is known to be an isolated VO_4 tetrahedra (20, 22). Thus, we can assume that the presence of a band at around 270–290 nm is indicative of isolated tetrahedral V^{5+} sites.

The DR spectra of calcined VAPO-5 samples with different vanadium contents are shown in Fig. 10. Quite similar spectra are obtained for samples with V content up to 2.5 wt%, with no bands with appreciable intensity in the 260–300-nm region. By increasing the vanadium content in VAPO-5, i.e., samples 2.5-C4 and 6.4-C10, some changes are observed in the DR spectra (Figs. 10f and 10g, respectively), which show some features in the 300–340-nm region (polymeric VO_4 tetrahedron) and a broad band in the 350–450-nm region, suggesting that some polymeric vanadium species (probably V_2O_5-like) is present.

As it has been observed from the thermogravimetric results, the calcined VAPO-5 samples are rapidly hydrated. For this reason, DR spectra of calcined samples were recorded immediately after drying at 200°C for 16 h. DR spectra of uncalcined, calcined, and dehydrated 0.5-D and 2.0-C4 samples (Figs. 11A and 11B, respectively) have been compared. In the uncalcined state, the sample 2.0-C4 gives two bands in the 550–800 nm-region, which are assigned to *d–d* transitions in VO^{2+} (20, 37, 38), once more supporting the incorporation of V^{4+} into the crystals. These bands disappear after calcination, indicating that V^{4+} has been mostly oxidized to V^{5+}.

In the case of the sample 0.5-D, obtained from V^{5+}-containing gel, the presence of V^{4+} species in the uncalcined sample is not detected by this technique. The band at ca. 280 nm suggests that vanadium incorporates, preferably, as tetrahedral V^{5+} species. For the calcined sample defined bands are not observed, indicating a change in the coordination of vanadium atoms. In addition to this, the presence of a band in the 270–300-nm region in the partially dehydrated samples (spectra c in Figs. 11A and 11B) can be noted. The presence of this band indicates the existence of tetrahedral V^{5+} species, suggesting that removal of water molecules changes the coordination of vanadium atoms from octahedral or square pyramidal to tetrahedral coordination. The influence of water on vanadium-related sites on the coordination of vanadium atoms has been also proposed for supported vanadium catalysts (24, 40, 41).

Different spectra are obtained for AlPO-5 supported vanadium samples (Fig. 12). These samples give a peak at 290 nm suggesting tetrahedral environment for V^{5+} and a second band at around 410 nm, which can be tentatively attributed to polymeric forms of vanadium (22) probably like in V_2O_5. Furthermore, this hypothesis is supported by the detection of a band at 1020 cm^{-1}, characteristic of V_2O_5 in the infrared spectra of the V/AlPO-5 samples (spectrum not shown).

EPR spectra. Figure 13 shows the EPR spectrum of the uncalcined 2.0-C4 sample evacuated at room temperature. The spectrum is consistent with an axially symmetric species with hyperfine structure due to the interaction of the $3d^1$ unpaired electron of V^{4+} with the magnetic nuclear moment of ^{51}V ($I = \frac{7}{2}$, 99.76% naturally abundant). This interaction gives rise to the splitting of the $g_\perp$ and $g_\parallel$ components into eight lines each (Fig. 13). The g values and the hyperfine constants are $g_\perp = 1.99$ (±0.01), $A_\perp = 80$ G (±5 G); $g_\parallel = 1.937$ (±0.005), $A_\parallel = 195$ G (±5 G). The perpendicular transition is generally less well resolved in the spectra and, thus, the corresponding error margins are larger. The EPR spectral parameters are in agreement with VO^{2+} in a square pyramidal or distorted octahedral environment (12, 16, 17, 22, 42–45). The site symmetry is usually described as C_{4v} with four V–O bonds in the equatorial plane and the vanadyl oxygen axially bonded along the z axis; a sixth ligand may lie opposite the vanadyl oxygen on the negative z axis (42–44). The hyperfine structure of the EPR signal is well resolved with a practically horizontal base line and no superimposed broad singlet is observed in the spectra, indicating that poly-

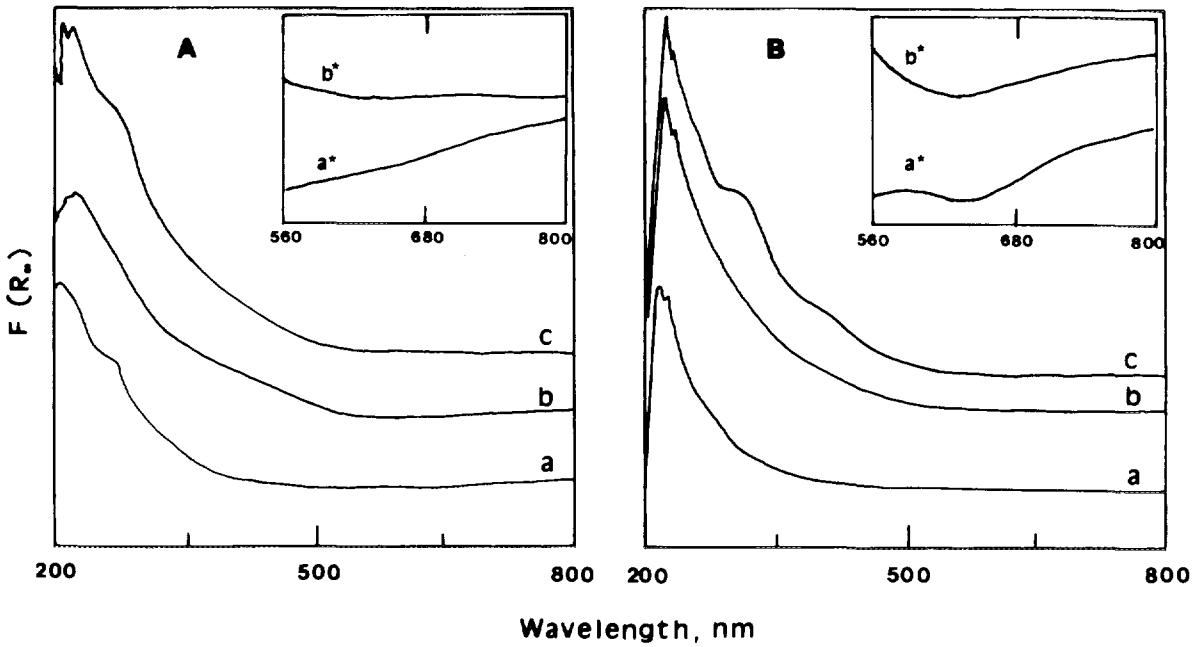

FIG. 11. DR spectra of uncalcined (a), calcined (b), and dehydrated (c) samples: (A) 0.5-D and (B) 2.0-C4.

meric V^{4+} species are not present and that VO^{2+} are isolated in the material.

Comparison of our V^{4+} EPR signals with those reported in previous studies on VAPO-5 shows that the spectral parameters are similar to the ones found by Rigutto and van Bekkum (16) and Jhung *et al.* (13), and slightly different from the values observed by Montes *et al.* (12) and Whittington and Anderson (17). In this same sense, only slightly different g and hyperfine constant values have been reported for V–silicalite (22). Centi *et al.* (22) attributed this signal to isolated VO^{2+} species in a distorted octahedral environment, probably placed inside the zeolitic channels and near OH groups. These hydroxy groups would be formed by the presence of vanadium during the hydrothermal synthesis or by the interaction of vanadium with the silicalite structure. This assignment was made on the basis of previous results reported for samples obtained by solid state reaction of V_2O_5 and H–ZSM5 (46).

A careful inspection of the outermost parallel components ($m_I = -\frac{7}{2}, -\frac{5}{2}$) of the EPR spectrum in Fig. 13 shows the presence of a second hyperfine signal which is not sufficiently well resolved to allow the determination of the anisotropic g and hyperfine constant tensors unambiguously. However, the $g_\parallel$ and $A_\parallel$ components are tentatively estimated to be $g_\parallel = 1.940$ and $A_\parallel = 185$ G. The presence of two hyperfine signals has been previously observed in VAPO-5 and attributed to two unequivalent vanadium sites (12, 16, 17). A doublet hyperfine structure

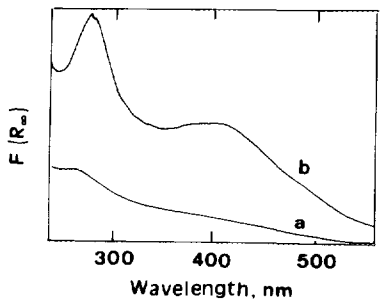

FIG. 12. DR spectra of $ALPO_4$-5 supported vanadium samples with 0.8 (a) and 2.2 (b) wt% of V atom.

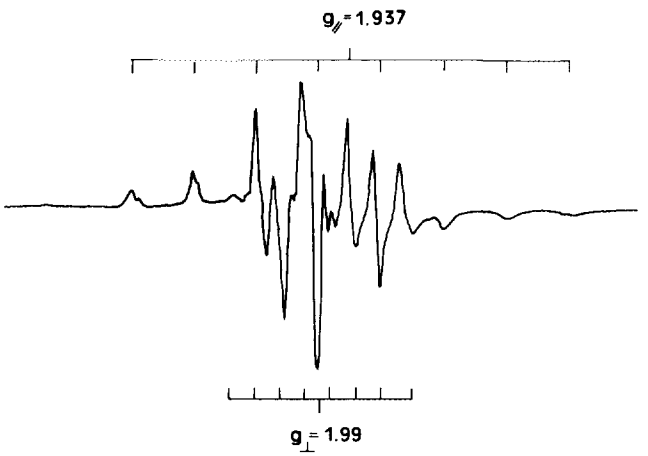

FIG. 13. EPR spectrum of uncalcined 2.0-C4 sample.

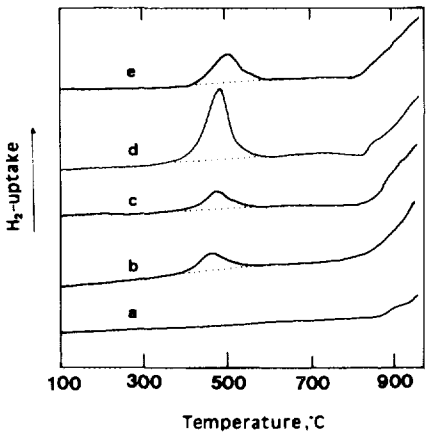

FIG. 14. TPR–H_2 results of VAPO-5 and V/ALPO samples: (a) $ALPO_4$-5, (b) 0.5-D, (c) 0.4-A, (d) 2.5-C4, and (e) 0.8V/ALPO.

was also detected in V–silicalite by Centi *et al.* (22) as a broadening of the low field parallel components and it was not possible to calculate the parameters. Nevertheless, it was tentatively attributed to the same type of coordinatively saturated vanadyl species mentioned above, but unsaturated due to the removal of coordination water. In our case, we find the presence of different vanadium sites with the same type of coordination as the most probable explanation for the appearance of this second signal.

Calcined sample gives a spectrum similar to that shown in Fig. 13 but with a much lower intensity. This indicates that although most of V^{4+} are oxidized to diamagnetic V^{5+}, there is still some V^{4+} after calcination. On the other hand, the presence of V^{4+} was also detected in the as-prepared 0.5-D sample synthesized from V^{5+}, strongly suggesting that some vanadium has been incorporated as V^{4+} in the aluminophosphate framework.

Temperature Programmed Reduction

Temperature programmed reduction (TPR) results of VAPO-5 and V/ALPO-5 samples are shown in Figure 14.

The VAPO-5 samples show, in general, two steps of hydrogen consumption. The maximum of the first step appears at about 470–475°C and its area increases with the vanadium content. The H_2 consumption associated to this peak is about 50% of the hypothetical hydrogen necessary to achieve a total $V^{5+} \rightarrow V^{3+}$ reduction. In Table 5 are indicated the H_2 consumption associated to the peak at 470°C from which it can be concluded that a first reduction, $V^{5+} \rightarrow V^{4+}$, occurs at this temperature. The second peak, which is observed at temperatures higher than 800°C, may be associated with the formation of a reduced compound during the thermal decomposition of the molecular sieve, as has been observed in other MeAPO-5 (47). From the fact that the area associated to this peak increases when increasing the vanadium content, it is possible to propose that $V^{4+} \rightarrow V^{3+}$ reduction occurs only in this temperature interval.

In the case of ALPO-5 supported vanadium samples two peak are also observed. The maximum of the first peak appears at a slightly higher temperature (about 490°C) with respect to VAPO-5. From the amount of hydrogen associated to this peak (Table 5) it can also be concluded that a partial $V^{5+} \rightarrow V^{4+}$ reduction occurs.

The fact that in VAPO-5 a partial reduction ($V^{5+} \rightarrow V^{4+}$) occurs may be explained on the basis of the stability of the V^{4+} species in the $ALPO_4$-5 structure. Jhung *et al.* (13) observed that the EPR spectrum of calcined VAPO-5 sample has a very low spin concentration (about $\frac{1}{40}$) compared with that of uncalcined VAPO-5, concluding that after calcination the V^{4+} species are mostly oxidized to V^{5+}. In addition to this, they observed that the reduction of calcined VAPO-5 samples with hydrogen or organic molecules at 450–500°C leads to V^{4+}, in agreement with our results. This V^{4+} species is easily restored as V^{5+} species by oxidation at 500°C (13).

On the other hand, it has been observed in MeAPO-5 samples (Me = Co, Zn, and Mn) that the reducibility of the metal takes place at temperatures higher than in the corresponding oxide due to the requirement of the previous collapse of the molecular sieve framework. This fact is consistent with the tetrahedral substitution of Co, Zn, or Mn in the molecular sieve framework (47).

In the case of VAPO-5 samples, $V^{5+} \rightleftarrows V^{4+}$ redox process occurs while the crystallinity is not affected. However, the $V^{4+} \rightarrow V^{3+}$ reduction is possible only with a collapse of the molecular sieve. The $V^{5+} \rightarrow V^{4+}$ reduction has also been observed on V–silicalite (22) or supported (SiO_2 or Al_2O_3) vanadium samples (48).

Catalytic Results

The catalytic results obtained during the oxidative dehydrogenation of propane on vanadium aluminophosphate samples are shown in Table 6. Propene, CO, and CO_2 were the main products obtained, while ethane and methane were detected only as traces at high reaction

TABLE 5

H_2-TPR Results Obtained on VAPO-5 and V/ALPO-5 Samples

Sample	Temperature (°C)	H_2 consumption (10^4 mol g^{-1})	V content (10^4 mol g^{-1})	Reduction degree (α)[a]
0.5-D	455	0.33	0.92	0.36
0.38-A	470	0.45	0.75	0.60
1.6-C5	475	1.49	3.10	0.48
0.8V/ALPO-5	490	0.75	1.57	0.48

[a] Considering $\alpha = 1$ for a total V^{5+} to V^{3+} reduction.

TABLE 6

Oxidative Dehydrogenation of Propane on VAPO-5 Catalysts

Sample	W/F^a	Temperature (°C)	Conversion (%)	Selectivity (%)			r_{C3H6} (10^3 mol h^{-1} g^{-1})^b
				C_3H_6	CO	CO_2	
0.38-A	47	520	21	64	24	12	2.85
		540	26	58	28	14	3.21
1.0-A	79	520	24	38	46	16	1.15
		540	31	29	52	19	1.14
1.4-B2	79	520	35	32	49	19	1.42
		540	47	24	54	22	1.43
2.5-C4	47	500	28	24	60	16	1.43
		520	45	15	67	18	1.44
1.6-C5	79	520	23	42	45	13	1.22
		540	27	35	52	13	1.20
0.5-D	65	520	18	63	23	14	1.74
		540	24	55	30	15	2.03
$ALPO_4$-5	175	540	4.2	97	0	3	0.23

[a] Contact time, W/F, in g_{cat} h (mol C_3H_8)$^{-1}$, where W is the weight of the catalyst exposed to the air (losses of 15 wt% of water are observed by TG results).

[b] Formation rate of propene.

temperature and high conversion levels of propane. Oxygenated products other than carbon oxides were not detected. $ALPO_4$-5 shows a lower activity than VAPO-5 samples, suggesting that the active sites in VAPO-5 could be related to vanadium species.

Figure 15 presents the variation of the initial rate for the conversion of propane with the vanadium content of VAPO-5 samples, obtained at 475°C and conversions of propane lower than 10%. Except in the case of the 1.6-C5 sample (1.59 wt% of vanadium in Fig. 15) a linearity between activity and vanadium content is observed.

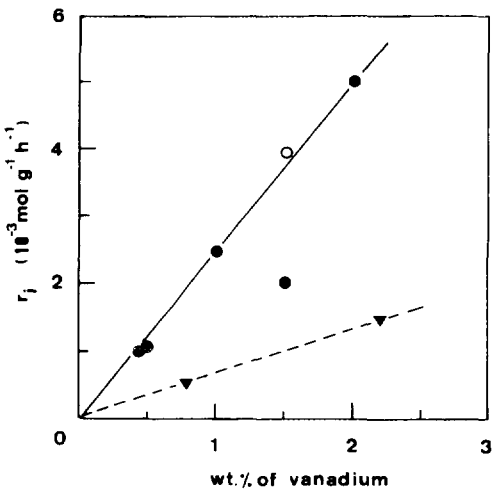

FIG. 15. Variation of the initial rate for the conversion of propane with the vanadium content of VAPO-5 (●), V/$ALPO_4$-5 (▼), and 1.6-C5-I (○) samples.

The presence of amorphous solids or the formation of V_2O_5 crystallites can modify the catalytic properties of these materials. In order to eliminate extraframework vanadium species, the 1.6-C5 sample was washed with ammonium (1.6-C5-I sample) or tetraethylammonium (1.6-C5-II sample) acetate aqueous solutions. The characteristic and catalytic properties of the resulting samples are shown in Table 7. It can be seen that the samples treated with acetate solutions (independently of the method used) present a higher activity although the vanadium content has practically not varied after washing. The fact that the linearity obtained in Fig. 15 is also observed for both 1.6-C5-I and 1.6-C5-II indicates that the presence of extraframework phases results in a decrease of activity.

The variation of the selectivities to propene, CO, and CO_2 with the propane conversion obtained during the ODH of propane on the 0.5-D sample is shown in Fig. 16. The higher the conversion of propane the lower the selectivity to propene is. This effect is independent to the reaction temperature interval (500–540°C) as it has been observed in other supported vanadium catalysts (6, 19, 20, 49).

The influence of propane conversions on the selectivity to propene obtained on different VAPO-5 samples, in the temperature range 500–540°C, is presented in Fig. 17. It can be seen that the highest selectivity to propene is obtained on samples with vanadium content lower than 0.5 wt%. A further increase of the metal content leads to a decrease of the selectivity.

The variation of the selectivities to CO and CO_2 with the variation of the vanadium content of VAPO-5 samples

TABLE 7

Characteristics and Catalytic Properties of Pure and Treated 1.6-C5 Samples

Sample	Vanadium (wt%)[a]	Crystallinity (%)[b]	Conversion (%)[c]	Selectivity (%)[c]			r_{C3H6} (10^3 mol h^{-1} g^{-1})[d]
				C_3H_6	CO	CO_2	
1.6-C5	1.59	56	27	35	52	13	1.45
1.6-C5-I[e]	1.53	32 + T	45	31	49	20	2.15
1.6-C5-II[f]	1.45	62	48	29	51	20	2.14

[a] In wt% of V atoms.
[b] Crystallinity of calcined samples are referred to uncalcined ALPO-5; *T*, trydimite.
[c] Obtained at a reaction temperature of 540°C and a contact time, *W/F*, of 65 $g_{cat}h$ (mol $C_3H_8)^{-1}$. *W* is the weight of the catalyst exposed to the air (losses of 15 wt% of water are observed by TG results).
[d] Formation rate of propene.
[e] Obtained from the treatment of the sample 1.6-C5 with an ammonium acetate solution.
[f] Obtained from the treatment of the sample 1.6-C5 with a tetraethylammonium acetate solution.

obtained at a conversion of propane of 30% is presented in Fig. 18. It can be noted that, while the selectivity to CO_2 is similar for all catalysts, the selectivity to CO rapidly increases with the vanadium content.

On the other hand the catalytic results obtained on $ALPO_4$-5 supported vanadium catalyst are presented in Table 8. The activity increases with the vanadium content. When the initial rates obtained on supported catalysts are compared with the data obtained on VAPO-5 samples (Fig. 15) it can be concluded that a higher intrinsic activity for vanadium atom is obtained on VAPO-5 samples. In addition to this, the selectivity to propene is lower on V/ALPO samples than on VAPO-5 samples.

DISCUSSION

Vanadium Incorporation into AFI Structure

Besides the crystallinity of the as-made crystals, the stability of V-containing $ALPO_4$-5 upon calcination in air has been proven to be a good test to determine the synthesis conditions suitable to obtain highly selective ODH catalysts. Particularly, fluoride anions and excess of acid should be avoided in the synthesis mixture, although the influence of pH is not yet clear to us.

In the samples keeping high crystallinity after calcination, the presence of protonated triethylamine compensating framework charge can be taken as a proof that vanadium isomorphous substitution in the AFI structure occurs. From the variation of the *a* parameter with the

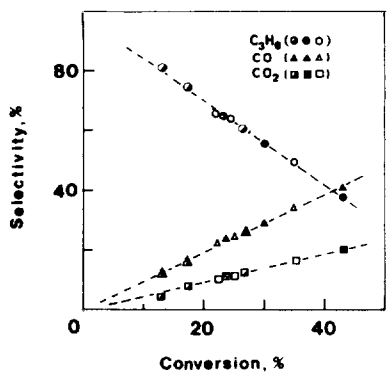

FIG. 16. Variation of the selectivities to propene, CO, and CO_2 with the propane conversion obtained for the oxydehydrogenation of propane on the 0.5-D sample at 500 (○, △, □), 525 (◑, ◭, ◪), and 550°C (●, ▲, ■).

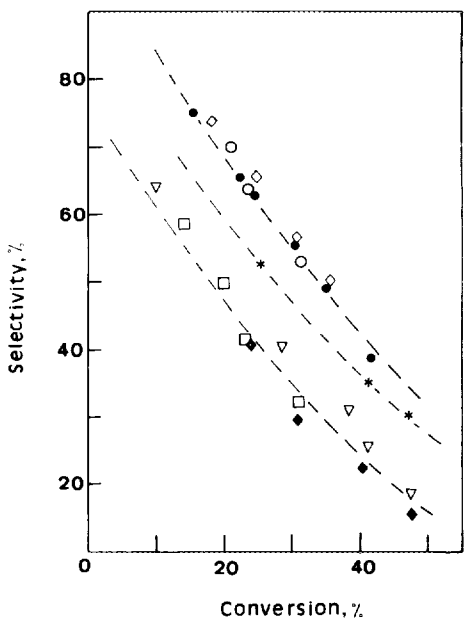

FIG. 17. Variation of the selectivity to propene with the propane conversion obtained during the oxidative dehydrogenation of propane, in the temperature range 550–550°C, on different vanadium aluminophosphates: 0.38-A (◇), 0.41-A (○), 1.4-B2 (▽), 2.5-C4 (◆), 1.65-C5 (□), 0.5-D (●), and 1.6-C5-I (*).

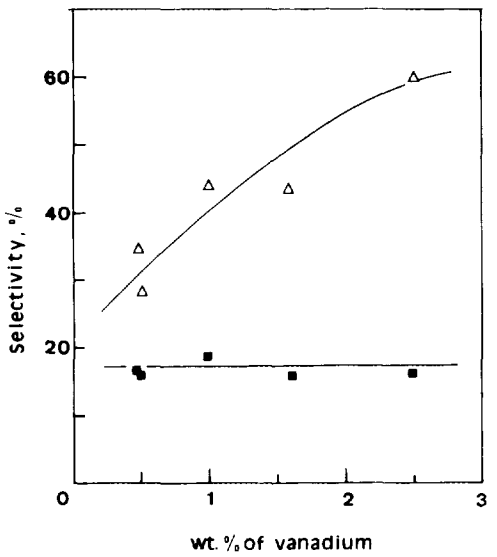

FIG. 18. Variation of the selectivities to CO (△) and CO_2 (■) with the vanadium content of VAPO-5 samples obtained at 550°C and a onversion of propane of 30%.

vanadium content (Fig. 2), an increase of ~0.1 Å per V atom is obtained. The EPR and DR data indicate that isolated vanadyl VO^{2+} species in 5 or 6 coordination are incorporated into the crystals, and no free tetrahedral V^{4+} species seems to exist. The V–O distances for 5- or 6-coordinated VO^{2+} range from 2 to 2.3 Å (43), several tenths of an Ansgtrom higher than the average P–O (1.5 Å) or Al–O (1.7 Å) distances. In this way, the average *T*–O–V bond angles (where *T* could be P or Al) should be strongly deformed to accommodate such long V–O distances, without strongly modifying the unit cell parameters.

TGA data suggest that the amount of organic compounds accompanying the V atoms located in the framework changes from about two for low vanadium contents to close to one for high vanadium loadings. Then, the existence of vanadium species of the type

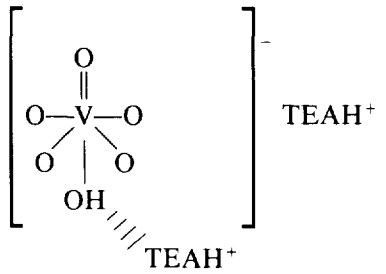

can be proposed for low vanadium contents. The sixth OH ligand could be replaced by a water molecule for high vanadium loading.

The above scheme implies the substitution of Al^{3+} by $(VO)^{2+}$. Although on experimental bases we cannot exclude the replacement of P atoms by VO^{2+}, the extremely high charge imbalance would make it rather unlikely. The hypothetical P substitution by V^{4+} ion should be feasible, but only VO^{2+} species are actually detected by EPR and DR in all ranges of vanadium contents. The two signals detected by EPR might correspond to vanadyl coordinated either by OH or H_2O molecules.

The need for the vanadium present in the framework to be associated to triethylamine might give a clue for the observed limit of ~1 V atom per unit cell. The maximum metal level attainable should correspond to the number of triethylamine that can be accommodated in the channel per unit cell, 1.6 molecules, slightly higher than the limit of vanadium. The TEA/V ratio equal to ~ 2 for crystals with low vanadium contents must account for that difference, and the same could also be true for VAPO-5 with high vanadium contents if the same ratio applies for the atoms incorporated into the crystals at the beginning of crystallization.

TABLE 8

Catalytic Properties of $ALPO_4$-5 Supported Vanadium Catalysts

Sample	*W/F*	Temperature (°C)	Conversion (%)[a]	Selectivity (%)			r_{C3H6} (10^3 mol h^{-1} g^{-1})[b]
				C_3H_6	CO	CO_2	
0.8V/ALPO	175	500	15	46.7	34.7	18.5	0.40
	175	540	39	27.7	53.1	19.2	0.62
2.2V/ALPO	175	500	30	42.6	42.7	14.7	0.73
	87	500	20	51.8	36.4	11.8	1.19
	87	540	39	31.6	51.4	17.0	1.42

[a] Contact time, *W/F*, in g_{cat} h (mol $C_3H_8)^{-1}$, where *W* is the weight of the catalyst exposed to the air (losses of 15 wt% of water are observed by TG results).

[b] Formation rate of propene.

Vanadium Sites and Catalytic Behavior

Calcination in air of crude crystals eliminates the organic and leaves the AFI structure basically untouched, provided the composition of synthesis gel is within the range discussed in the preceding section. During calcination, vanadyl groups are oxidized to V(V) species, as is shown by H_2 reduction of calcined materials, although some V(IV) ions still remain, as is shown in the EPR spectra of calcined samples. Provided that the oxidized metal atoms keep, at least partially, their bondings to the framework, isolated V(V) centers are expected after oxidation. The V(V) atoms removed from the framework will polymerize to give V_2O_5. This compound is observed only in the samples with vanadium contents higher than 1 V/u.c. However, octahedral V(V) species are detected by NMR in all samples. According to all experimental evidence, this species should correspond to $V(O)_4(H_2O)_2$. Indeed, partial water removal allows the detection of tetrahedrally coordinated V(V) by DR. The expansion of the coordination shell of Al from 4 to 6 by hydration in VAPO-5 is clearly demonstrated by MAS NMR (Fig. 8), as has also been shown for pure $ALPO_4$-5 (28, 35). The charge to radii ratio is even higher for V(V) than for Al, as well as its ionic radii, and then also the hydration of V(V) could be feasible.

It has been claimed that isolated VO_4 tetrahedron is the active and selective site for the oxidative dehydrogenation of propane (4, 6, 7–10, 19, 49). In our case, the tetrahedral coordination of vanadium should be restored after desorption of water at $T > 200$°C. Indeed, the VAPO-5 catalysts here reported are highly selective for the oxidative dehydrogenation of propane. As was discussed before, the nature of vanadium centers does not change up to 1 V/u.c., and then a linear relationship between ODH activity and vanadium content in this interval can be anticipated. This is what actually takes place (Fig. 15). Indeed, the ALPO-5 supported catalysts, where extraframework V_2O_5 is observed, are much less active. However, it can be also observed that despite the constancy in specific activity, the selectivity to propene decreases when the vanadium content increases (Fig. 17). Diffusional restrictions of propene through the channels, which would increase the true residence time of the molecule and, consequently, its oxidation to CO and CO_2, cannot be argued to explain the effect, as the crystal size remains practically constant (~ 1 μm) in all the catalysts studied here. Therefore, it can be concluded that the increase of the metal site density itself renders more likely the propene readsorption into these sites and its conversion to carbon oxides.

This study leaves open the question of the influence of the nearest tetrahedral neighbors of vanadium on its catalytic behavior. Unmistakable experimental proofs are not yet available to determine whether P–O–V or Al–O–V bonds (or both) exist in vanadium-substituted $ALPO_4$-5 and if this has any influence on its catalytic activity. Comparison of the present data with those of high-silica vanadium zeolites would help not only to clarify this point, but also to design a better catalyst for selective ODH of short chain paraffins.

CONCLUSIONS

The amount of V incorporated into the ALPO-5 framework and the stability of VAPO-5 upon calcination are strongly influenced by the preparation procedure. VAPO-5 samples with vanadium content higher than 3 wt% show low crystallinity, and after calcination dense aluminophosphate phase (trydimite) and V_2O_5 are formed. Crystalline VAPO-5 is also obtained when F^- anions are presented in the synthesis gel, but it shows a low crystallinity after calcination. The incorporation of vanadium atoms in the framework is favored when the synthesis is carried out from V^{4+} instead of V^{5+}. The vanadium atoms are incorporated as isolated vanadyl VO^{2+} ions in square pyramidal or distorted octahedral environments. The $TEAH^+/V$ ratio changes from 2 to 1 when the vanadium content increases.

After calcination in air, most of the V^{4+} ions are oxidized to V^{5+}, which are in square pyramidal or octahedral symmetry, but envolve toward tetrahedral upon dehydration, probably due to the loss of one or two extra water molecules in the coordination shell of vanadium. Extraframework polymeric vanadium species are detected in calcined samples with vanadium content higher than 2.5 wt%.

The VAPO-5 samples are active and selective catalysts for the oxidative dehydrogenation of propane. Both the activity and selectivity obtained on these materials are higher than on $ALPO_4$-5 supported vanadium catalyst. In VAPO-5, the activity increases linearly with the vanadium content up to ~ 2 wt% of vanadium. Isolated tetrahedral V^{5+} species are proposed to be the active and selective sites for the oxidative dehydrogenation of propane.

ACKNOWLEDGMENT

Financial supports by Comisión Interministerial de Ciencia y Tecnología in Spain (MAT 607/91) is acknowledged.

REFERENCES

1. Gellins, P., *in* "Catalysis" (G. C. Bond and G. Webb, Eds.), Specialist Periodical Reports, Vol. 7, p. 105. Royal Society of Chemistry, London, 1985.
2. Bond, G. C., and Tahir, S. F., *Appl. Catal.* **71,** 1 (1991).
3. Oyama, S. T., *Res. Chem. Intermed.* **15,** 1965 (1991).
4. Chaar, M. A., Patel, D., and Kung, H. H., *J. Catal.* **109,** 463 (1988).
5. Siew Hew Sam, D., Soenen, V., and Volta, J. C., *J. Catal.* **123,** 417 (1990).

6. Corma, A., López Nieto, J. M., and Paredes, N., *J. Catal.* **144,** 425 (1993).
7. Corma, A., López Nieto, J. M., Paredes, N., Pérez, M., Shen, Y., Cao, H., and Suib, S. L., *in* "New Development in Selective Oxidation by Heterogeneous Catalysis" (P. Ruiz and B. Delmon, Eds.), Studies in Surface Science and Catalysis, Vol. 72, p. 213. Elsevier, Amsterdam, 1992.
8. Zatorski, L. W., Centi, G., López Nieto, J. M., Trifiró, F., Bellusi, G., and Fattore, V., *in* "Zeolites: Facts, Figures, Future" (P. A. Jacobs and R. A. van Santen, Eds.), Studies in Surface Science and Catalysis, Vol. 49, p. 1243. Elsevier Amsterdam, 1989.
9. Bellussi, G., Centi, G., Perathoner, S., and Trifiró, F., in "A.C.S. Symposium Series," Vol. 523, p. 281. American Chemical Society, Washington, 1993.
10. Concepción, P., López Nieto, J. M., and Pérez-Pariente, J., *Catal. Lett.* **19,** 333 (1993).
11. Flanigen, E. M., Lok, B. M., Patton, R. L., and Wilson, S. T., *in* "New Development in Zeolite Science and Technology" (Y. Murakami, A. Iijima, and J. W. Ward, Eds.), Studies in Surface Science and Catalysis, Vol. 28, p. 103. Elsevier, Amsterdam, 1986.
12. Montes, C., Davis, M. E., Murray, B., and Narayama, M., *J. Phys. Chem.* **94,** 6431 (1990).
13. Jhung, S. H., Uh, Y. S., and Chon, H., *Appl. Catal.* **62,** 61 (1990).
14. Kornatowski, J., Sychev, M., Baur, W. H., and Finger, G., *Collect. Czech. Chem. Commun.* **57,** 767 (1992).
15. Miyamoto, A., Iwamoto, Y., Matsuda, H., and Inui, T., *in* "Zeolites: Facts, Figures, Future" (P. A. Jacobs and R. A. van Santen, Eds.), Studies in Surface Science and Catalysis Vol. 49, p. 1233. Elsevier, Amsterdam, 1989.
16. Rigutto, M. S., and van Bekkum, H., *J. Mol. Catal.* **81,** 77 (1993).
17. Whittington, B. I., and Anderson, J. R., *J. Phys. Chem.* **97,** 1031 (1993).
18. Hong, S. B., Hwang, B. W., Yeom, Y., Kim, S. J., and Uh, Y. S., *in* "Chemistry of Microporous Crystals" (T. Inui, S. Namba, and T. Tatsumi, Eds.), Studies in Surface Science and Catalysis, Vol. 60, p. 179. Elsevier, Amsterdam, 1991.
19. Corma, A., López Nieto, J. M., Paredes, N., and Pérez, M., *Appl. Catal.* **97,** 159 (1993).
20. Corma, A., López Nieto, J. M., and Paredes, N., *Appl. Catal.* **104,** 161 (1993).
21. Minchev, C., Minkov, C., Penchev, V., Weda, H., and Lechert, H., *J. Therm. Anal.* **37,** 171 (1991).
22. Centi, G., Perathoner, S., Trifiró, F., Aboukais, A., Aissi, C. F., and Guelton, M., *J. Phys. Chem.* **96,** 2617 (1992).
23. Occelli, M. L., Maxwell, R. S., and Eckert, H., *J. Catal.* **137,** 36 (1992).
24. Eckert, H., and Wachs, J. S., *J. Phys. Chem.* **93,** 6796, (1989).
25. Lapina, O. B., Simakov, O. A. V., Mustikhin, V. M., Veniaminov, S. A., and Shubin, A. A., *J. Mol. Catal.* **50,** 55 (1989).
26. Lapina, O. B., Mustikhin, V. M., Simonova, L. G., and Bulkagova, Y. O., *J. Mol. Catal.* **69,** 61 (1991).
27. Lapina, O. B., Nosov, A. V., Mustikhin, V. M., Dubkov, K. A., and Mokrinski, V. V., *J. Mol. Catal.* **87,** 57 (1994).
28. Jelinek, R., Chmelka, B. F., Wu, Y., Davis, M. E., Ulan, J. G., Gronsky, R., and Pines, A., *Catal. Lett.* **15,** 65 (1992).
29. Blackwell, C. S., and Patton, R. L., *J. Phys. Chem.* **92,** 3965 (1988).
30. Zibrowius, B., Löffler, E., Finger, F., Sonntag, E., Hunger, M., and Kornatowski, J., *in* "Catalysis and Adsorption by Zeolites" (G. Ohlmann, H. Pfeifer, and R. Fricke, Eds.), Studies in Surface Science and Catalysis, Vol. 65, p. 537. Elsevier, Amsterdam, 1991.
31. Franco, M. J., Pérez-Pariente, J., Blasco, T., and Sanz, J., *Zeolites* **12,** 386 (1992).
32. Zibrowious, B., Lohse, U., and Richter-Mendau, J., *J. Chem. Soc., Faraday Trans.* **87**(9), 1433 (1991).
33. Blackwell, C. S., and Patton, R. L., *J. Phys. Chem.* **88,** 6135 (1984).
34. Martens, J. A., Janssens, C., Grobet, P. J., Beyer, H. K., and Jacobs, P. A., *in* "Zeolites: Facts, Figures, Future" (P. A. Jacobs and R. A. van Santen, Eds.), Studies in Surface Science and Catalysis, Vol. 49, p. 215. Elsevier, Amsterdam, 1989.
35. Goepper, M., Guth, F., Delmotte, L., Guth, J. L., and Kessler, H., *in* "Zeolites: Facts, Figures, Future" (P. A. Jacobs and R. A. van Santen, Eds.), Studies in Surface Science and Catalysis, Vol. 49, p. 857. Elsevier, Amsterdam, 1989.
36. Appleyard, I. P., Harris, R. K., and Fitch, F. R., *Chem. Lett.*, 1747 (1985).
37. Grange, P., and Harris, R. K., *in* "Multinuclear Magnetic Resonance in Liquids and Solids—Chemical Applications," p. 299. Kluwer Academic Publishers, Netherlands, 1990.
38. Lischke, G., Hanke, W., Jerchkewitz, H. G., and Öhlmann, G., *J. Catal.* **91,** 54 (1985).
39. Hanke, W., Bienert, R., and Jerchkewitz, H. G., *Z. Anorg. Allg. Chem.* **414,** 109 (1975).
40. Went, G. T., Oyama, S. T., and Bell, A. T., *J. Phys. Chem.* **94,** 4240 (1990).
41. Owens, L., and Kung, H. H., *J. Catal.* **144,** 202 (1993).
42. Sharma, V. K., Wokaun, A., and Baiker, *J. Phys. Chem.* **90,** 2715 (1986).
43. Nowinska, K., and Wiechowski, A. B., *Z. Phys. Chem. (Munnich)* **162,** 231 (1989).
44. Chary, K. V. R., Reddy, B. M., Nag, N. K., Subrahmanyam, S., and Sumandana, C. S., *J. Phys. Chem.* **88,** 2622 (1984).
45. Che, M., Canosa, B., and Gonzalez-Elipe, A. R., *J. Phys. Chem.* **90,** 618 (1986).
46. Sass, C. E., Chen, X., and Kevan, L., *J. Chem. Soc., Faraday Trans.* **86,** 189 (1991).
47. Roque-Malherbe, R., López-Cordero, R., Gonzales-Morales, J. A., Oñate-Martinez, J., and Carreras-Gracial, M., *Zeolites* **13,** 481 (1993).
48. Erdöhelyi, A., and Solimosi, F., *J. Catal.* **123,** 31 (1990).
49. Corma, A., López Nieto, J. M., Paredes, N., Dejoz, A., and Vazquez, M. I., *in* "New Developments in Selective Oxidation II" (V. Cortés and S. Vic, Eds.), Studies in Surface Science and Catalysis, Vol. 82, p. 113. Elsevier, Amsterdam, 1994.